Molecular Stress and Strain in an Oriented Extended-Chain Polymer of Finite Molecular Length

M.-C. G. Jones and D. C. Martin*

Department of Materials Science and Engineering, The University of Michigan, Ann Arbor, Michigan 48109-2136

Received February 10, 1995[⊗]

ABSTRACT: We have developed constitutive and molecular mechanics models to investigate the influence of chain-end defects on the macroscopic tensile properties of extended-chain polymers of finite molecular weight. Molecular mechanics simulations have been performed on the rigid-rod polymer PBZO, poly(*p*-phenylene benzobisoxazole), using the Dreiding II force field. The distance between chain ends (i.e., the chain length) can be varied systematically by increasing the size of the simulation unit cell in the chain direction. From this analysis it is possible to analyze the micromechanics of stress transfer between chains in detail. At chain ends, the applied tensile stress is transferred to the nearby chains through a shear lag region via secondary bonds. A constitutive model is developed for a geometry similar to the PBZO molecular simulations. The calculated strain distribution along individual chains describes well the strain distribution along the PBZO molecules. The model predicts a nonlinear response of the material and a transition in tensile failure mode from chain slip to chain scission, which depend on the interchain shear strength and the length of the polymer molecules. The influence of intermolecular shear modulus, shear strength, and molecular chain length on macroscopic properties such as tensile modulus, tensile strength, and elongation to break is examined. It is found that in the molecular engineering of strong, tough polymer fibers, an optimum combination of shear strength and chain length must be chosen.

(1) Introduction

The concept of fully extended-chain polymers was advanced by Staudinger more than 60 years ago.[1] The development of lyotropic liquid crystalline fibers which can be dry-jet wet spun into highly oriented fibers has made it possible to closely approach this limit.[2] As a result of their extended molecular configuration, these fibers possess very high tensile moduli (≈200 GPa) and tensile strengths (≈4 GPa).[2] Extended-chain polymers include the aromatic polyamides such as poly(*p*-phenyleneterephthalamide) (PPTA or commercial name Kevlar), aromatic copolyesters of *p*-hydroxybenzoic acid (HBA) and 2-hydroxy-6-naphthoic acid (HNA), and the rigid-rod polymers poly(*p*-phenylenebenzobisoxazole) (PBZO) and poly(*p*-phenylenebenzobisthiazole) (PBZT). Extended-chain polymers have been the subject of intense characterization efforts. The main element of the structure is an oriented microfibrillar network formed upon coagulation of the liquid-crystalline fiber.[3] The microstructure of extended-chain polymers such as PBZO has been studied in detail.[4]

A complete theoretical treatment of the tensile deformation of extended-chain polymers is an enormous task because of the complexity of the structure. Molecular simulation gives information on the molecular scale of the deformation of single molecules or of a perfect three-dimensional array of molecules. In this case the structural characteristics of the material are not considered. Only a theoretically perfect crystal elastic modulus may be obtained. Similarly, techniques such as Raman spectroscopy, X-ray diffraction, and pulse propagation techniques only determine the crystal lattice modulus.[5,6] Efforts have been directed toward developing simple constitutive models that predict the macroscopic tensile deformation and fracture behavior of extended-chain polymers using their structural characteristics and theoretical mechanical properties. We review some of the existing models. A special emphasis is then made on structural models and deformation models related to the presence of chain-end defects.

Northolt and Hout described the dependence of the elastic properties on the orientation distribution of the crystallites.[7] In this series model, the fiber is regarded as being built up of parallel aligned fibrils in which crystallites having a narrow orientation distribution relative to the fiber axis are linked end to end. The elastic extension of the fibrils results from the elastic stretching of the polymer chains and from the shear deformation induced crystallite rotation. For this model it is shown that the modulus E is given by

$$1/E = 1/E_c + \langle \sin^2 \varphi_o \rangle / 2G$$

where E_c is the chain or sonic modulus, $\langle \sin^2 \varphi_o \rangle$ is the orientation parameter, and G is the shear modulus. The equation for the stress σ–strain ϵ curve of the fiber with well-oriented chains is

$$\epsilon = \epsilon_{stretch} + \epsilon_{rotation} = \sigma/E_c + {}^1/_2\langle \sin^2 \varphi_o \rangle [1 - \exp(\sigma/G)]$$

Allen et al. derived similar equations by considering the coupling between axial loading and shearing deformation.[8] The relationship for the modulus variation during deformation is

$$1/E = 1/E_a + [\langle \tan^2 \varphi_o \rangle / G] \exp(-2\sigma/G)$$

where E_a is the asymptotic modulus at high stress. The stress–strain equation obtained by integration is

$$\epsilon = \sigma/E_a + [\langle \tan^2 \varphi_o \rangle / 2][1 - \exp(-2\sigma/G)]$$

Penning et al. developed a simple morphological model for high molecular weight polyethylene, of microfibrils consisting of an almost infinite sequence of crystalline blocks interrupted by disordered domains.[9] Taut tie molecules (TTM) form the connections between

* To whom correspondence should be addressed.

[⊗] Abstract published in *Advance ACS Abstracts,* August 15, 1995.

0024-9297/95/2228-6161$09.00/0

adjacent crystalline blocks. According to this model, sample failure will occur when the TTM in the disordered domains are stressed to fracture. The strength of the fiber is

$$\sigma_f = \beta\sigma_{th}$$

where β is the fraction of TTM in the disordered domains and σ_{th} represents the theoretical strength of the chain. The modulus of the fiber is

$$E = E_o[1 + (L_d/L_c)]/[1 + (1/\beta)(L_d/L_c)]$$

where E_o is the theoretical modulus and L_d/L_c is the ratio of the length of the disordered domain to the length of the crystalline blocks in the microfibril. L_d/L_c may be calculated from the crystallinity χ and is given by

$$L_d/L_c = (1 - \chi)/(\chi - \beta)$$

Shuppert presented a model for the transport of defects to explain the creep of oriented high-modulus fibers.[10] He derived equations for the elastic modulus of two parallel chains. If one of the chains is pulled to one side and the other to the other side, then the tensile modulus E is

$$E = 2E_o(f \sinh f)(f \sinh f + \cosh f)$$

where E_o is the chain elastic tensile modulus, $f = L(2\mu)^{1/2}$, $\mu = G_o/(E_oX^2)$, $2L$ is the length of the chains, G_o is the interchain shear modulus, and X is the interchain distance. Alternatively, if only one chain is pulled but in both directions, the tensile modulus of the two chains model becomes

$$E = 2E_o(f \cosh f)(f \cosh f + \sinh f)$$

Martin has introduced "intermolecular twist defects" representing local physical entanglements between chains that are likely to be present at the gain boundary phase area between crystallites.[11] The modulus of the twisted bundle, E, is found to decrease with respect to that of the untwisted reference state, E_o, as follows:

$$E/E_o = 1/(1 + (1 + \nu)/\tan^2 \alpha)$$

where ν is the Poisson ratio and α is the angle of twist.

All the above models relate the polymer's macroscopic deformation behavior to microstructural characteristics. Structural models and deformation models related to the presence of chain ends resulting from finite molecular weight are presented in the next paragraphs.

Predecki and Statton showed the importance of chain-end defects on the structure of crystalline polymers.[12] Four simple types of line defect can be generated by chain ends: screw and edge dislocations and coupled-screw and coupled-edge dislocations. The coupled-screw and coupled-edge dislocations are shown to be more energetically favorable than screw and edge dislocations. A random arrangement of chain ends in an otherwise perfect molecular arrangement may disorder the structure sufficiently to make it appear "amorphous". Examples of defects are given, including clusters of chain ends, chain ends which are condensed into line defects, and boundaries between misaligned crystalline regions.

Morgan et al. described the deformation and failure processes of PPTA fibers as controlled primarily by chain-end concentration and chain-end distribution within the fiber.[13] Their proposed structural model particularly emphasizes the chain-end distribution. The macromolecules are assumed to be aligned parallel to the fiber axis, with the chain ends on the fiber exterior arranged essentially randomly relative to one another and becoming progressively more clustered in the fiber interior. The clustering results in periodic weak planes every 200 nm, or average PPTA macromolecular length, along the fiber axis. This chain-end model makes it possible to explain the experimentally observed fracture surface of Kevlar 49 without involving macromolecular chain scission. As emphasized by the authors, chain scission and molecular pullout also occur during the failure of PPTA fibers.

Bartenev et al. have presented an analysis of the theoretical strength of polymers in a completely oriented state by accounting for the intermolecular interaction and finite length of polymer chains.[14] In the model, the stretched macromolecules represent a planar zigzag, similar to polyethylene. The macromolecules are joined at the ends by dispersion bonds which are the weakest links in the structure. Intermolecular interactions are continuously distributed along the macromolecular length. The elastic deformation of the whole macromolecule is determined by the deformation angles. However, the destruction of the structure occurs first by rupture of the dispersion bonds between the ends of the macromolecules, then by slippage or by rupture of the macromolecules themselves depending on the molecular weight and molecular interactions. Numerical evaluation of the theoretical strength of fully oriented Kapron shows that the theoretical strength is practically independent of the degree of polymerization. This means that at all molecular weights in fully oriented Kapron, the rupture of the macromolecules occurs without their slippage. The authors emphasize the importance of the intermolecular interaction.

Termonia et al. have theoretically studied the influence of the molecular weight and the influence of the anisotropy between intrachain and interchain forces on the fiber strength.[15-17] These studies consider the case of ideal fibers made of a perfectly ordered array of fully extended macromolecules, with no defects other than chain ends. The approach is based on the kinetic theory of fracture in which the bond ruptures are simulated by a Monte Carlo process on a three-dimensional array of nodes. The covalent bonds are represented by strong bonds between nodes in one dimension, and the weak interchain secondary bonds are represented by weak bonds between nodes in the other two dimensions. For polyethylene fibers, the authors find a gradual change in the failure process from slippage involving rupture of secondary bonds at low molecular weight to chain fracture as well as secondary bond rupture at high molecular weight.[15] For PPTA, a high concentration of stress rapidly starts to build up due to the high concentration of chain ends resulting from the small number of PTA units per macromolecules. As a result, catastrophic failure is initiated through rupture of the macromolecules themselves.[16] The effect of chain end segregation on the tensile deformation behavior of PPTA and polyethylene is explored.[17]

In a recent study, Termonia described the effects of fiber size and polymer molecular weight on chain-end segregation extent.[18] The model focuses on the limiting case of maximum possible segregation. For a monodisperse molecular weight, it is found that the lateral

extent of the coupled chain-end aggregates is proportional to the fiber diameter, above a certain fiber size. Polydispersity however leads to a significant decrease in the size of the aggregates. A majority of single coupled chain-end defects is observed for reasonable values of fiber diameter to chain length ratio and of polydispersity index. A strong tensile strength/fiber diameter relationship is found for monodisperse chain length distribution, whereas a much weaker relationship is observed for polydisperse chain length distribution.

Yoon has developed a theory of the tensile strength of highly oriented fibers and compares its results with existing tensile strength data of HBA/HNA thermotropic copolyester fibers.[19] The fiber structure is assumed to be a short fiber composite in which the reinforcing fibers are the polymer chains. It is assumed that the fiber breakage occurs when the interchain interaction force, e.g. the shear stress, exceeds a critical value. Both the chain length distribution and the chain orientation effects are included in the model. The authors find an excellent fit between the experimental tensile strength values and the tensile strength calculated using a most-probable chain length distribution. Introducing the effect of orientation distribution leads to very little change in the calculated strength. Yoon concludes that the tensile strength increase upon heat treatment of HBA/HNA aromatic polyester fibers is mostly due to a molecular weight increase resulting from transesterification. This is suggested from the tensile strength of both as-spun and heat-treated fibers being predicted with a single shear strength. However this is not relevant for PPTA and PBZO since no intermolecular reactions are expected in these materials during heat treatment. Yoon points out that the increase in tensile strength observed upon heat treatment of Kevlar fibers may result from an increased shear strength. Another conclusion is that the fiber stress–strain behavior should be essentially elastic and thus reversible. This conclusion is based on the bonded length at fracture being 10 times larger than the average chain length.

In the present work, the deformation behavior of polymers in a perfectly oriented state is studied by taking into account the intermolecular interactions and molecular weight of the macromolecules. We use molecular modeling to follow the strain distribution along individual molecules and to show the effect of chain-end density on the theoretical tensile modulus. We develop our own constitutive model to describe the stresses on a single macromolecule of finite length in an oriented extended-chain polymer, as well as to evaluate the general deformation behavior and mode of failure of the polymers. We predict mechanical properties such as tensile strength and strain to failure as a function of intermolecular shear strength, intermolecular shear modulus, and chain length. Throughout this paper, comparisons of the present approach and Yoon's approach and comparisons of the present results and Termonia et al.'s results are made.

(2) Molecular Simulation of Chain-End Defects: Procedure

The simulations were made using the Polygraf and CERIUS software packages of Molecular Simulations Inc., using triply periodic conditions and the default settings of Dreiding II force field, except for the convergence criteria (RMS force in (kcal/mol)/A and RMS gradient in (GPa/A) set at 0.005). We used PBZO molecules rather than PPTA molecules because PBZO has a less developed three dimensional nature as well as no hydrogen bonds. The total energy as a function of shifting between PBZO molecules shows less pronounced minima than in the case of PPTA. As a result the simulations for PBZO are less computationally intensive. In addition, PBZO is more appropriate for comparison with our constitutive model, which assumes uniform interaction between continuous molecules. A two-chain PBZO periodic unit cell was created using the draw facility of Polygraf and minimized. The elementary unit cell of size c, in the z or molecular axis direction was then extended using CERIUS into two, four, eight, and sixteen unit cells, of lengths $2c$, $4c$, $8c$, and $16c$. Chain ends were introduced into each extended unit cell and the simulations were minimized in Polygraf.

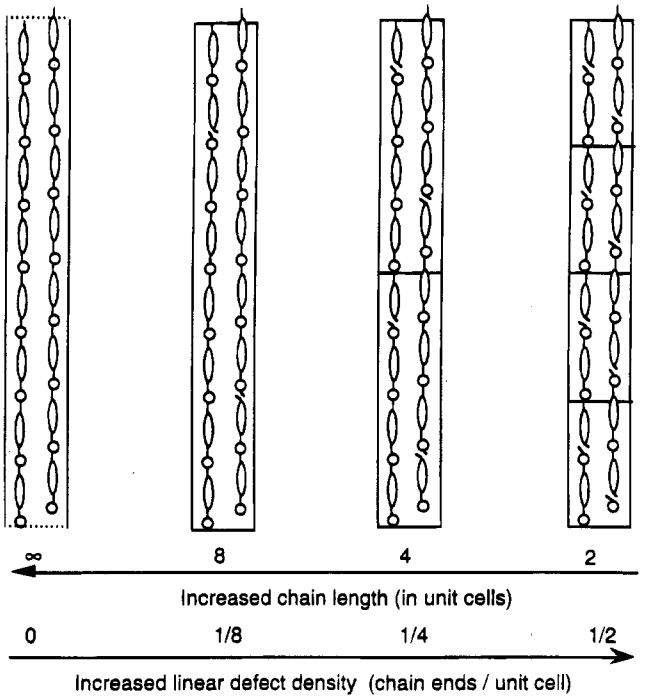

Figure 1. Schematic of the simulations of various lengths.

The coupled chain-end defects were created by cutting a C–C single bond connecting the benzene ring to the heterocyclic group and attaching a hydrogen atom at each end. This procedure introduces a compressive strain (*relaxation strain*) near the chain ends. The extent and implication of this relaxation strain are discussed further. The ability to increase the length of the simulation in the chain direction makes it possible to systematically increase the length or molecular weight of the molecules, e.g. decrease the density of the coupled chain-end defects. Figure 1 is a schematic of the simulations of various lengths. The linear defect densities are 0 for infinitely long molecules to 0.0625 unit cell^{-1} for the biggest simulation of 16 cells.

In order to determine the influence of chain ends on mechanical tensile properties, stresses of 0.25–1 GPa were applied in the z direction. The lengths of the extended unit cells were recorded to calculate tensile moduli. The coordinates of the carbon atoms shown by arrows on Figure 2 were obtained from CERIUS and were used to calculate the tensile strains ϵ_i along the chain 1. *Relaxation strains* resulting from the small size of the voids between chain ends were determined by comparing the simulations containing defects to the simulation of the unit cell representative of infinitely long PBZO molecules. *Mechanical strains* were determined by comparing the simulations prior to and after applying the external load.

(3) Molecular Simulation of Chain-End Defects: Results

Figure 3 shows the minimum energy configuration of PBZO, as minimized by Polygraf. The PBZO structure has been previously studied by Martin and Thomas.[11,20] The laterally associated neighboring molecules are

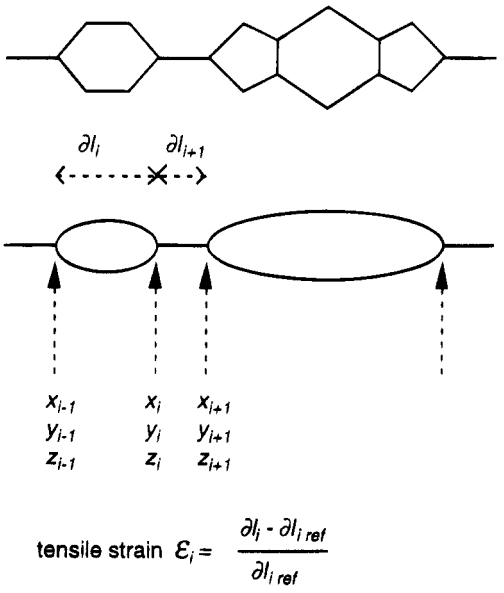

Figure 2. Schematic of the PBZO molecules. The atomic coordinates used to define the strains are indicated by arrows.

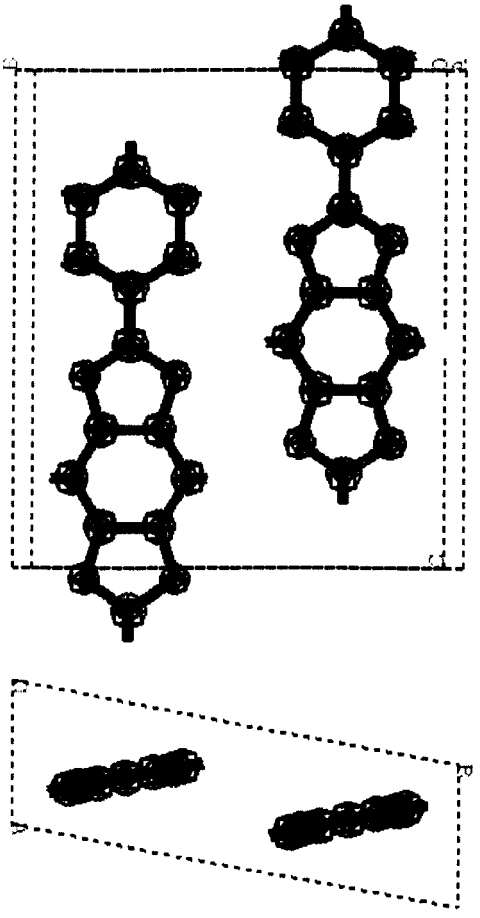

Figure 3. Minimum energy configuration of the PBZO crystal structure.

displaced by $\pm 1/4$ with respect to one another. The benzene rings and heterocyclic groups are nearly coplanar. The optimum unit cell parameters are $a = 0.3548$ nm, $b = 1.1938$ nm, $c = 1.2166$ nm, $\alpha = 90.003°$, $\beta = 89.997°$, and $\gamma = 79.275°$. These are comparable to the cell parameters obtained with an earlier version of the Dreiding II force field.[11]

The *relaxation* strain distribution along a molecule of a 16-cell simulation is plotted in Figure 4. The strain

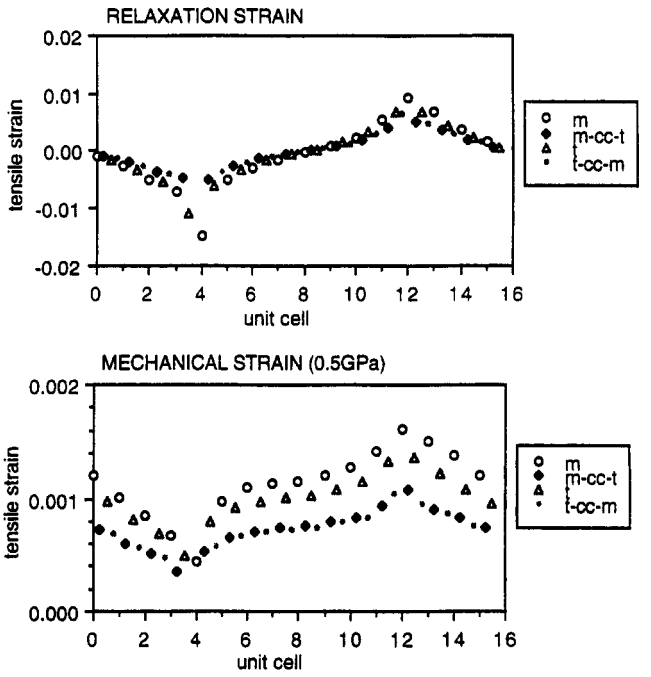

Figure 4. *Relaxation* and *mechanical* strain distribution for a 16-cell simulation. The relaxation strain results from the geometry of the simulations. The mechanical strain results from the 0.5 GPa applied tensile stress.

is plotted for each unit: the benzene ring denominated by m for "mono-ring", the heterocyclic group denominated by t for "tri-ring", and the carbon–carbon single bonds cc. The molecules are in local compression near the ends and in local tension where the ends belong to the nearby chain. Our procedure for creating the chain ends is responsible for the observed relaxation of the ends due to repulsive interactions between the hydrogens. This was verified by minimizing an 8*c* extended unit cell containing voids of length one unit cell. In this case no relaxation strain was observed.

The *mechanical* tensile strain distribution for a 16-cell simulation is also shown in Figure 4 for an applied stress of 0.5 GPa (average tensile strain of 0.000 95). Different curves are apparent for the different units of the molecules, emphasizing the heterogeneity of the local stiffness along the molecule. The units in order of increasing stiffness are the benzene rings (m), the heterocyclic groups (t), and the carbon–carbon single covalent bonds (cc) which deform the least. The various stiffnesses of the moieties along the backbone of extended-chain polymers have been shown before.[21] Wierschke performed a molecular deformation analysis of various polymers in tension by examining changes in the lengths and angles of units such as the phenyl moiety, the heterocyclic moiety, and carbon–carbon bonds connecting the two groups.[21] He used the results to explain the different moduli and strengths exhibited by various molecular structures.

The strain distribution along the molecule indicates that stress transfer occurs in a shear-lag region at the molecular ends. The strain is close to zero near the chain end, and the stress is necessarily transferred to the nearby molecules. The strain builds up to the average applied strain along the length. The highest strain is found where the chain ends are in the nearby chains and cannot carry their share of the applied load. Thus at the chain ends, the applied tensile load is transferred through intermolecular bonds via a shear-lag mechanism. The observed stress transfer mecha-

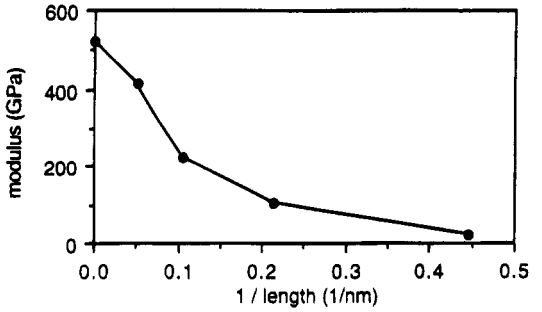

Figure 5. Tensile modulus as a function of chain length.

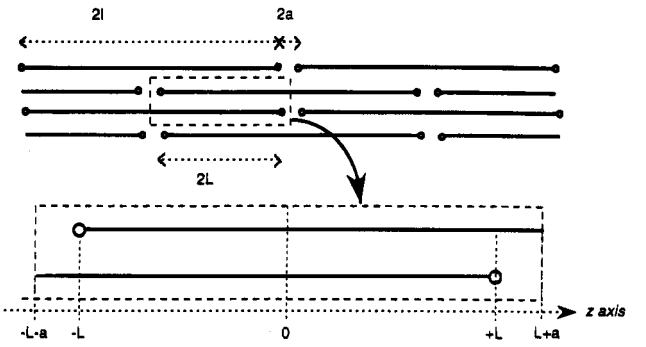

Figure 6. Two-dimensional model employed for the constitutive model.

nism is similar to the mechanism observed in discontinuous fiber composites and is the basis of our constitutive model.

Local molecular deformation in organic fibers has been investigated with Raman spectroscopy. For a wide variety of high-performance fibers, the Raman bands shift to different wavenumbers on the application of strain, indicating that mechanical deformation leads directly to molecular deformation in the fiber.[22-25] Various studies have shown the applicability of Raman spectroscopy in measuring the stress distribution of individual reinforcement fibers in composites.[26-28] For single fibers in a matrix, the shear-lag analysis proposed by Cox provides an analytical solution of the fiber load distribution.[29] No spectroscopy technique presently exists that has the resolution to measure the local stress distribution along individual molecules.

The elastic modulus decreases with the chain-end defect density, as shown in Figure 5. A coupled chain-end defect every eight unit cell or every 10 nm on all the chains decreases the modulus by more than half. However this result should not be interpreted too quantitatively. Due to the small size of the voids, a small proportion of the tensile stress may be transferred at the chain ends, increasing the modulus. Also, an externally applied tensile stress may relieve the relaxation strain in addition to deforming the extended unit cell, thus lowering the apparent modulus. Future work needs to be done to investigate the effect of the size of the voids. The decrease in modulus with coupled chain-end density should be taken as an expected trend. The load transfer capabilities may become even more important in real extended-chain fibers where the macromolecular length is of the order of 100 nm, but where the chain ends may be segregated.[12]

(4) Constitutive Model: Analysis

As shown by the molecular modeling results, an oriented polymer of extended molecules of finite length may be considered as a microcomposite in which the molecules are bonded to one another through secondary bonds. The stress concentrations in a composite and the stress transfer process at fiber ends have been studied extensively.[30-32] Here we use a continuum approach: the molecules of discrete atoms and finite length are assumed to be discontinuous fibers. We apply the concepts of engineering composite mechanics to calculate the local strain distribution along the molecules and the stress–strain curves. We compare the theoretical results to the molecular mechanics results and predict a transition in failure mechanism from chain slip to chain scission with increased intermolecular bond strength or with longer polymer chains. We also use this model to assess the influence of intermolecular shear strength, intermolecular shear modulus, and chain length on the fiber elastic and ultimate tensile properties.

The following approximations are made in the present work. The molecules carry an applied tensile load σ. Stress transfer is made only through a shear-lag region via secondary bonds; e.g. no tensile load is transferred at the molecular ends. Normal stresses in the transverse directions are neglected. The molecular chains behave perfectly elastically in tension, with an intrinsic molecular tensile modulus E_0, up to their intrinsic tensile strength σ_f. The interchain shear stress–strain curve is composed of an elastic region of shear modulus G_0, and a plastic region. Intermolecular debonding occurs as a result of the rupture of the weak secondary bonds, when the shear stress τ reaches the intrinsic shear strength τ_0. The debonded interface supports a shear stress of τ_0. Thus two local modes of failure exist, namely local interchain debonding (when $\tau \geq \tau_0$) and chain scission (when $\sigma \geq \sigma_f$).

The model employed, shown in Figure 6, is two-dimensional and is similar to the geometry of the molecular simulations for which all the (a, c) planes are identical. As the chains are regularly arrayed in this model, the equations for stress equilibrium are given for the representative elementary region surrounded by the broken line. The center of this region is taken at $z = 0$. The geometrical features of the model are the length of the molecules, $2l$, the length of the voids between molecules, $2a$, the distance between the molecules in the transverse direction, X, and the transverse dimension of the molecules, D. The length of the "overlap region" is $2l = 1 - a$.

A schematic representation of the various deformation stages with increasing stress is shown in Figure 7. At low applied stresses, the interchain shear stress is purely elastic. As the applied stress is raised, debonding occurs first at the ends of the macromolecules at $z = \pm L$ where the shear stress is maximum and reaches the intrinsic shear strength ($\tau = \tau_0$). With a further increase of the applied stress, the debonded length increases and the elastic shear region is constrained within $-z_0 \leq z \leq z_0$. Failure occurs either by chain scission, when the maximum tensile stress on the chains reaches the intrinsic molecular tensile strength σ_f, or by chain slippage, when interchain debonding has occurred along the whole length of the superimposed macromolecule region. As a result of the symmetry of the model, the same occurs also in all other "elementary cells".

Yoon's assumptions for his fiber strength theory are somewhat different from the present assumptions.[19] Both the length distribution and the chain orientation are taken into account, respectively, by a most probable distribution and a Laurentz-IV distribution. The extended-chain polymer is assumed to be similar to a fiber

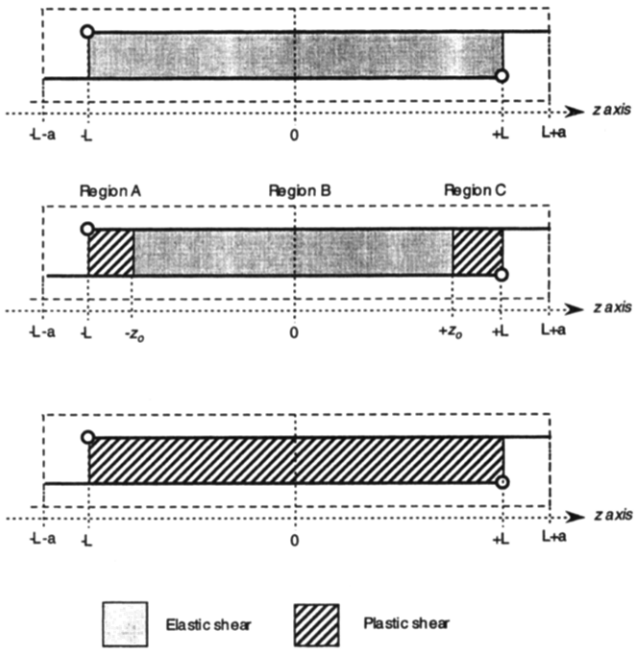

Figure 7. Schematic representation of the deformation stages.

composite, and the model is based on elastic load transfer between the chains and a matrix. Therefore the stress distribution on the chains is similar to the stress distribution along a fiber in a single fiber composite. This is not the case in the present model which assumes that the load transfer is made between neighboring chains through nonbonded interactions, and which does not require any hypothetical matrix.

Another major difference between Yoon's approach and the present approach resides in the value of the shear stress at the debonded interface.[19] Yoon assumes that the separated matrix/chain interface does not support any load. In this case the debonding phenomenon corresponds to a shortening of the "useful" chain length. Our assumption however is that the debonded interchain interface supports a maximum shear stress τ_o. For comparison purposes, calculations were made using a zero shear stress at the debonded interchain interface. For the model used here, it was found that such an assumption would lead to an instability at the onset of debonding; e.g. the debonded length would "decrease" (from zero) with an increasing applied stress.

Finally, Yoon does not use a simple chain fracture or chain slippage criteria to calculate the polymer tensile strength.[19] The chains are assumed to be infinitely strong; thus fiber failure cannot occur by simple chain fracture. The sum of the average tensile load on individual bridging chains with a "fracture zone" is considered. This fracture zone is a slice of the fiber representative of the entire fiber, containing ending chains and bridging chains (for which the ends are not within the fracture zone). The tensile strength is obtained by maximizing the total load with respect to the debond length value.

Equations of Stress Equilibrium. The equations of stress equilibrium are presented for the deformation stage containing both elastic and debonding shear regions. For simplicity the regions for $-L \le z \le -z_o$, $-z_o \le z \le z_o$, and $z_o \le z \le L$ are named regions A, B, and C, respectively. Two constants, characteristics of the parameters in the model and with dimensions of inverse length, are defined: $p = 2/D$ and $t = \sqrt{4G_o/XE_oD}$. Large values of p are obtained for narrow molecules, e.g. a high polymer density. Similarly, large values of t correspond to a low material anisotropy (high G_o/E_o ratio) and to a high polymer density (low XD). A, B, C_1, C_2, and C_3 are constants. The tensile stresses and displacements on chains 1 and 2 are respectively σ_1, σ_2 and u_1, u_2.

The forces applied on an element of chain 1 of length δz are $-\sigma_1 D^2$, $(\sigma_1 + \delta\sigma_1)D^2$, and $-2\tau D\delta z$. The stress equilibrium equations are

$$\frac{\delta\sigma_1 D^2 - 2\tau D\delta z}{D^2\delta z} = 0 \quad \text{on chain 1 or} \quad \frac{d\sigma_1}{dz} - p\tau = 0 \tag{1}$$

and

$$\frac{\delta\sigma_2 D^2 + 2\tau D\delta z}{D^2\delta z} = 0 \quad \text{on chain 2 or} \quad \frac{d\sigma_2}{dz} + p\tau = 0 \tag{2}$$

The basic equations

$$\sigma_1 = E_o\frac{du_1}{dz} \quad \text{and} \quad \sigma_2 = E_o\frac{du_2}{dz}$$

become by differentiating and inserting (1) and (2)

$$p\tau = E_o\frac{d^2u_1}{dz^2} \quad \text{and} \quad -p\tau = E_o\frac{d^2u_2}{dz^2} \tag{3}$$
(4)

For regions A and C, the shear stresses are

$$\tau_A = \tau_C = \tau_0 \tag{5}$$

so

$$\sigma_{1A} = p\tau_o z + C_1 \quad \text{for region A} \tag{6}$$

and

$$\sigma_{1C} = p\tau_o z + C_2 \quad \text{for region C} \tag{7}$$

For region B, the shear stress is defined by

$$\tau_B = G_o\frac{u_{1B} - u_{2B}}{X} \tag{8}$$

Differentiating this equation twice with respect to z and inserting (3) and (4) gives the following differential equation in τ:

$$\frac{d^2\tau_B}{dz^2} = \frac{2G_o p}{XE_o}\tau_B \quad \rightarrow \quad \frac{d^2\tau_B}{dz^2} - t^2\tau_B = 0 \tag{9}$$

General solutions for τ_B, σ_{1B}, and σ_{2B} are obtained from (9), (1), and (2):

$$\tau_B = A\exp(tz) + B\exp(-tz) \tag{10}$$

$$\sigma_{1B} = \frac{pA}{t}\exp(tz) - \frac{pB}{t}\exp(-tz) + C_3 \tag{11}$$

$$\sigma_{2B} = -\frac{pA}{t}\exp(tz) + \frac{pB}{t}\exp(-tz) + C_3 \tag{12}$$

Boundary Conditions and Solutions. The boundary conditions to solve the integral constants A, B, C_1, C_2, and C_3 and the length z_o are given as follows.

(a) At $z = 0$, $\sigma_{1B} = \sigma_{2B} = \sigma \rightarrow A = B$ and $C_3 = \sigma$, so (11) becomes

$$\sigma_{1B} = \frac{2pA}{t}\sinh(tz) + \sigma \qquad (11')$$

and (10) becomes

$$\tau_B = 2A\cosh(tz) \qquad (10')$$

(b) At $z = -L$, $\sigma_{1A} = 0 \rightarrow C_1 = p\tau_o L$, so (6) becomes

$$\sigma_{1A} = p\tau_o(z + L) \qquad (6')$$

(c) At $z = +L$, $\sigma_{1C} = 2\sigma \rightarrow C_2 = -p\tau_o L + 2\sigma$, so (7) becomes

$$\sigma_{1C} = p\tau_o(z - L) + 2\sigma \qquad (7')$$

(d) At $z = z_o$, $\tau_B = \tau_C = \tau_o$, so (10′) leads to $A = \tau_o/2\cosh(tz_o)$ and becomes

$$\tau_B = \tau_o\frac{\cosh(tz)}{\cosh(tz_o)} \qquad (10'')$$

and (11′) becomes

$$\sigma_{1B} = \frac{p}{t}\tau_o\frac{\sinh(tz)}{\cosh(tz_o)} + \sigma \qquad (11'')$$

(e) At $z = z_o$, $\sigma_{1B} = \sigma_{1C} \rightarrow (p/t)\tau_o\tanh(tz_o) + \sigma = p\tau_o(z_o - L) + 2\sigma$

$$tz_o - \tanh(tz_o) = tL - \frac{t}{p}\frac{\sigma}{\tau_o} \qquad (13)$$

Equation 13 giving z_o may be approximated by

$$tz_o - 1 \approx tL - \frac{t}{p}\frac{\sigma}{\tau_o} \qquad (13')$$

assuming that

$$tL - \frac{t}{p}\frac{\sigma}{\tau_o} \geq 1 \quad \text{or} \quad \sigma \leq \frac{p\tau_o}{t}(tL - 1) \qquad (14)$$

Thus for a given material and applied tensile stress, the shear stress and tensile stress (or strain) distribution along chain 1 are described by (5), (6′), and (7′) for regions A and C and (10″) and (11″) for the elastic region B. For $L \leq z \leq L + a$, $\sigma_1 = 2\sigma$ and $\tau = 0$, and for $-L - a \leq z \leq L$, $\sigma_1 = 0$ and $\tau = 0$. The length z_o of region B may be obtained by solving (13), or (13′) if approximation (14) is met. From the symmetry of the model the stresses on the rest of chain 1 at $z \geq L + a$ may easily be obtained through $\sigma_1(L + a + \epsilon) = \sigma_1(L + a - \epsilon)$ and $\tau(L + a + \epsilon) = -\tau(L + a - \epsilon)$.

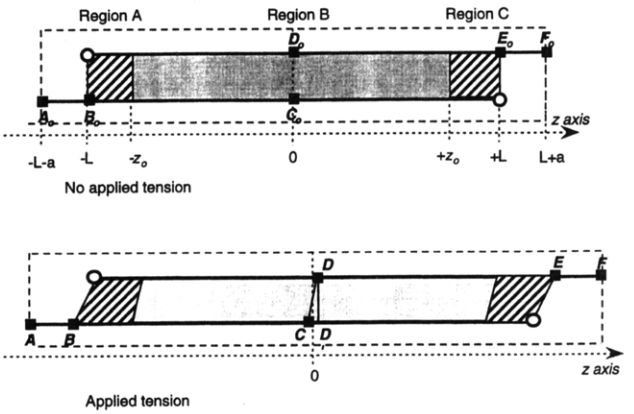

Figure 8. Schematic representation of the deformed model.

Finally, the tensile stresses on chain 2 are related to that on chain 1 by

$$\sigma_{2A}(z) = \sigma_{1C}(-z) = p\tau_o(-z - L) + 2\sigma \qquad (15)$$

$$\sigma_{2B}(z) = \sigma_{1B}(-z) = -\frac{p\tau_o}{t}\frac{\sinh(tz)}{\cosh(tz_o)} + \sigma \qquad (16)$$

$$\sigma_{2C}(z) = \sigma_{1A}(-z) = p\tau_o(-z + L) \qquad (17)$$

Stress-Strain Curves. The global tensile elastic modulus may be calculated using the elementary displacements along z for $-L - a \leq z \leq L + a$. The displacements u_1 and u_2 of chains 1 and 2 are given by

$$u_1(z) = \frac{1}{E_o}\int\sigma_1(x)\,dx + C^{ste} \quad \text{and} \quad u_2(z) = \frac{1}{E_o}\int\sigma_2(x)\,dx + C^{ste}$$

For example:

$$u_{1B}(z) = \frac{p\tau_o}{E_o t^2}\frac{\cosh(tz)}{\cosh(tz_o)} + \frac{\sigma}{E_o}z + C^{ste} \quad \text{from (11″)}$$

$$u_{1C}(z) = \frac{p\tau_o}{E_o}\left(\frac{z^2}{2} - Lz\right) + \frac{2\sigma}{E_o}z + C^{ste} \quad \text{from (7′)}$$

$$u_{2A}(z) = \frac{p\tau_o}{E_o}\left(-\frac{z^2}{2} - Lz\right) + \frac{2\sigma}{E_o}z + C^{ste} \quad \text{from (15)}$$

$$u_{2B}(z) = -\frac{p\tau_o}{E_o t^2}\frac{\cosh(tz)}{\cosh(tz_o)} + \frac{\sigma}{E_o}z + C^{ste} \quad \text{from (16)}$$

The general equation for the modulus is

$$E = \sigma\frac{\sum\text{length}}{\sum\Delta(\text{length})} \qquad (18)$$

with length $= \overline{A_oC_o} + \overline{D_oF_o} = 2L + 2a$ and $\Delta(\text{length}) = \Delta(\overline{AB}) + \Delta(\overline{BC}) + \overline{CD'} + \Delta(\overline{DE}) + \Delta(\overline{EF})$ (see Figure 8).

The changes in length are given by the following equations:

$$\Delta(\overline{AB}) = \Delta(\overline{EF}) = a\frac{2\sigma}{E_o}$$

$$\Delta(\overline{BC}) = [u_{2B}(0) - u_{2B}(-z_0)] + [u_{2A}(-z_0) - u_{2A}(-L)]$$

$$\overline{CD'} = \tau_B(z=0)\frac{X}{G} \equiv |u_{1B}(0) - u_{2B}(0)| = \frac{2p\tau_0}{E_0 t^2}\frac{1}{\cosh(tz_0)}$$

$$\Delta(\overline{DE}) = [u_{1C}(L) - u_{1C}(z_0)] + [u_{1B}(z_0) - u_{1B}(0)]$$

Equation 18 becomes

$$\frac{E}{E_0} = \frac{L+a}{(2a+2L-z_0) + \frac{\tau_0}{\sigma}\left(\frac{p}{t^2} - \frac{p(z_0-L)^2}{2}\right)} \quad (18')$$

Calculations. At low applied stresses for which only the elastic region B exists, the value for z_0 calculated from (13′) is larger than L. In this case z_0 should be given the value L, and (10″) and (11″) may be used to compute the stress distribution along the chains. Using $z_0 = L$, τ_0/σ obtained from (13) is $\tau_0/\sigma = \tau/(p\ \tanh(tL))$ and the elastic modulus (eq 18′) is

$$\frac{E}{E_0} = \frac{L+a}{L+2a+\frac{1}{t\ \tanh(tL)}}$$

Local debonding starts to occur at the chain ends when $z_0 = L$, or when the applied stress is $\sigma \approx p\tau_0/t$ (eq 13′)). At stresses slightly higher than $p\tau_0/t$, both the elastic B and the debonded regions A and C exist and $0 \le z_0 \le L$. z_0 may be calculated with (13′). As the applied stress is increased further to a level for which approximation 14 is wrong, e.g. just before the debond regions A and C cover the entire length of the chain, (13) should be used to numerically solve z_0. Equations 10″ and 11″ may be used to calculate the stress distribution along chain 1 for $-z_0 \le z \le z_0$, and (6′), (7′), and (5) may be used when $|z| \ge z_0$.

Material failure by slip occurs when all the length of the chains is debonded. Region B disappears for the critical z_0 value of 0. This will occur if failure by chain scission has not occurred yet. Failure by chain scission corresponds to the maximum tensile stress on the chain 2σ reaching the intrinsic molecular tensile strength σ_f, or $\sigma = \sigma_f/2$. Failure by slip occurs for $z_0 = 0$ which corresponds to an applied stress of $\sigma = p\tau_0 L$ (see (13)). At this critical stress, the stress distribution along chain 1 is easily computed from (5), (6′), and (7′). Equation 18′ gives the modulus.

(5) Constitutive Model: Results

Most of the parameters in the constitutive model were estimated from the molecular simulation results. The values for the geometrical features are as follows.

•Length of molecules ($2l$): typically 100.5 nm (variable).

•Length of voids between molecules ($2a$): 0.5 nm.

•Distance between molecules in the transverse direction (X): 0.28 nm, corresponding to $^1/_4$ of the b unit cell dimension.

•Transverse dimension of the molecules (D): 0.28 nm.

The molecular mechanical properties are as follows.

•Chain tensile modulus (E_0): 525 GPa. This is the value obtained from the second derivative of the energy potential by Polygraf on a periodic PBZO crystal.

•Interchain shear modulus (G_0): 9 GPa (variable). The shear moduli obtained from Polygraf are $G_{13} = 2.2$ GPa and $G_{23} = 9.5$ GPa. For our simulations, $G_{23} =$ 9.5 GPa is of interest since the load around chain ends is transmitted to the nearby chains primarily through secondary bonds in the b direction.

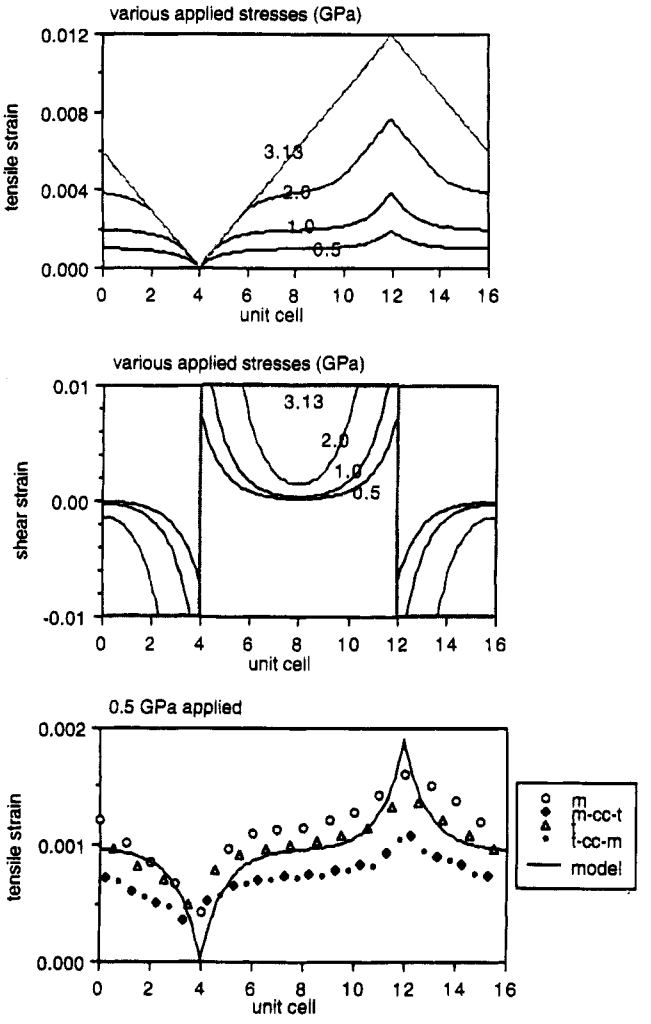

Figure 9. Computed tensile and shear strain distribution along chain 1, for various applied stresses. Comparison with the molecular simulation results is made in the last plot. (Shear modulus = 9 GPa, shear strength = 0.09 GPa, chain length = 19.2 nm or 16 unit cells.)

•Chain tensile strength (σ_f): 20 GPa (variable), which is consistent with the results of Kausch.[33] Kausch estimated the force which pulls a tie molecule out of a polyethylene (PE) and polyamide (PA) crystal. The maximum axial stress which a perfect PE or PA crystallite is able to exert on a tie molecule was found to be respectively 7.5 and 22.4 GPa. A 20 GPa stress is also consistent with a model developed by Termonia et al. which estimates the ultimate tensile strengths of extended and oriented PE and PPTA molecules respectively at 24 and 15 GPa.[15,16]

•Interchain shear strength (τ_0): 0.09 GPa (variable) or 1% of the shear modulus. Knoff measured the shear strength and the shear modulus for a variety of aramid fibers, the ratio of the two parameters being on average 0.05.[34]

The above values were used for all parameters unless otherwise stated. The variables are the chain length, the interchain shear modulus, and the interchain shear strength.

Figure 9 shows the tensile and shear strain along chain 1 of a region twice the size of the representative region of Figure 6, for various applied tensile stresses. The horizontal axis is shown in unit cells (16 unit cells

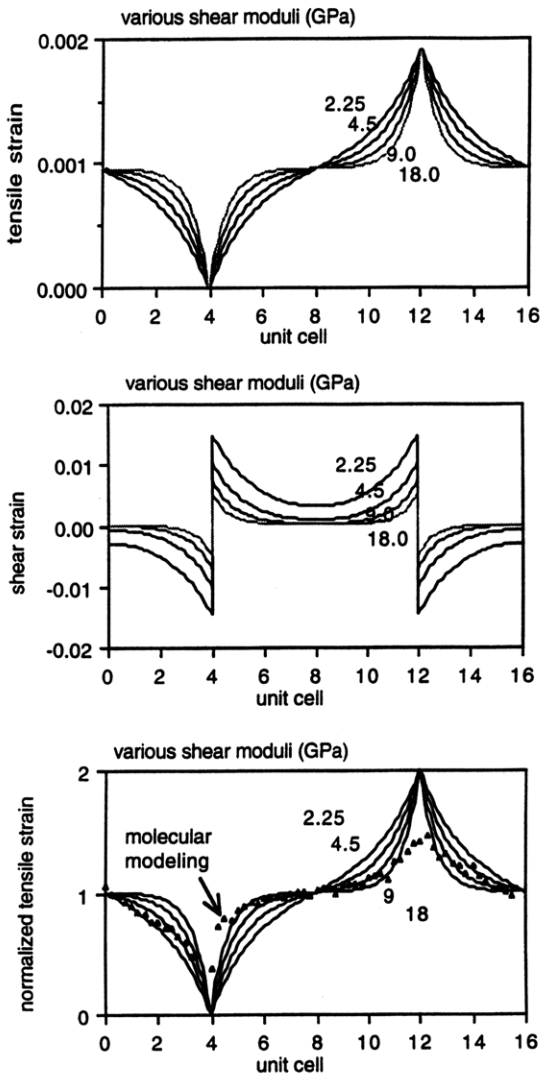

Figure 10. Computed tensile, shear, and normalized tensile strain distribution along chain 1, for various shear moduli. The applied stress is 0.5 GPa. (Shear strength = 0.09 GPa, chain length = 19.2 nm or 16 unit cells.)

or 19.2 nm) for comparison with the molecular simulation results of Figure 4, also displayed on the last graph. The highest applied stress, 3.13 GPa, is the stress leading to total debonding and therefore failure. The shape of the strain distributions obtained from molecular simulations and from the constitutive model are very similar, except perhaps at chain ends. The other difference arises from the continuum approach to describe the mechanical response of molecules of discrete atoms. Nevertheless, the theoretical calculation describes well the molecular modeling data, showing that elasticity theory may be applied down to the molecular level.

The shear and tensile strain distribution along chain 1 is shown for various shear moduli on Figure 10. The applied stress of 0.5 GPa is low enough for the interchain shear to remain elastic. Increasing the value of G_0 has a similar effect as increasing the length or aspect ratio of the chains: the stress is transferred at the chain ends over smaller fractions of the fiber length, and the maximum shear strain at the ends is lowered. The normalized tensile strain distributions, obtained from both the molecular simulations and the constitutive model, are illustrated in the last graph. Comparison of the theoretical curves with the simulation results

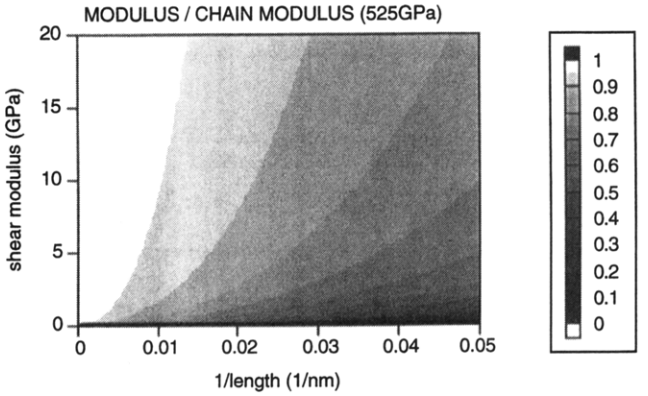

Figure 11. Computed normalized tensile modulus as a function of chain length and of shear modulus (zero applied stress, shear strength = 0.09 GPa).

demonstrates the suitability of a shear modulus of 9 GPa.

The elastic tensile modulus increases with higher interchain shear modulus and longer chains, as displayed in Figure 11. This results from the chains being fully stressed along a greater proportion of their lengths for greater shear moduli and chain lengths. The increase in tensile modulus with shear modulus is also described in the Allen and Roche equation outlined in the Introduction.[8] The drop in tensile modulus with decreased chain length is less important than the drop observed with the molecular simulations. A likely reason for this apparent discrepancy is the pre-existence of the *relaxation* strain, as mentioned before in the results section of molecular simulations. In Termonia et al.'s model, the modulus decreases with molecular weight for both PPTA and PE.[16,17] For a same molecular length, of 170 nm for example, the drop in modulus is greater for PPTA than for PE. This may be due to the lower number of PPTA molecules per unit surface area carrying the external load, namely a higher D and X (respectively dimension of molecule and intermolecular distance). Termonia explains the difference in modulus between PPTA and PE in terms of the number of secondary bonds per length of molecules, assumed to be proportional to the number of repeat units.[16]

When the applied tensile stress reaches a certain threshold, $\sigma \approx p\tau_0/t$, local interchain debonding takes place, starting at the chain ends where the shear stress is highest. It is possible to partition the microstructure of the polymer into three regions: the void, the length of chain submitted to elastic shear and the length of chain submitted to plastic shear or debonded from its neighbors. The evolution of this microstructure as a function of increased applied tensile stress is displayed on Figure 12 for a chain length $2l$ of 100.5 nm. The void increases in size with higher applied load. Plastic shear or debonding starts to occur for an applied stress of 0.7 GPa, and the debonded region grows at the expense of the elastic shear region until global failure occurs, in this particular case by chain scission for the applied stress of 10 GPa.

The graph of Figure 12 may be summarized by plotting the evolution of the elastic length z_0 with increased applied tensile stress. Figure 13 shows the variation of z_0 as a function of the applied stress for various chain lengths, shear strengths, and shear moduli. The original value of z_0 is $L = (2l - 2a)/4$ or a quarter of the chain length minus a quarter of the void length, for example 25.0 nm when the chain and void

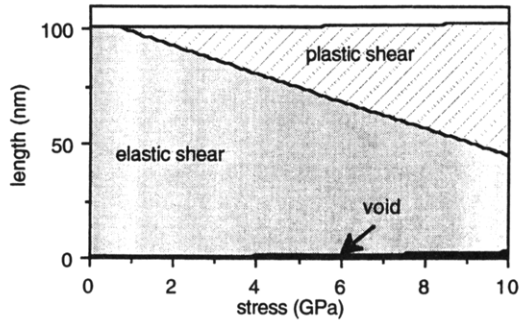

Figure 12. Micromechanics of deformation as a function of the applied tensile stress (shear modulus = 9 GPa, shear strength = 0.09 GPa, chain length = 100.5 nm).

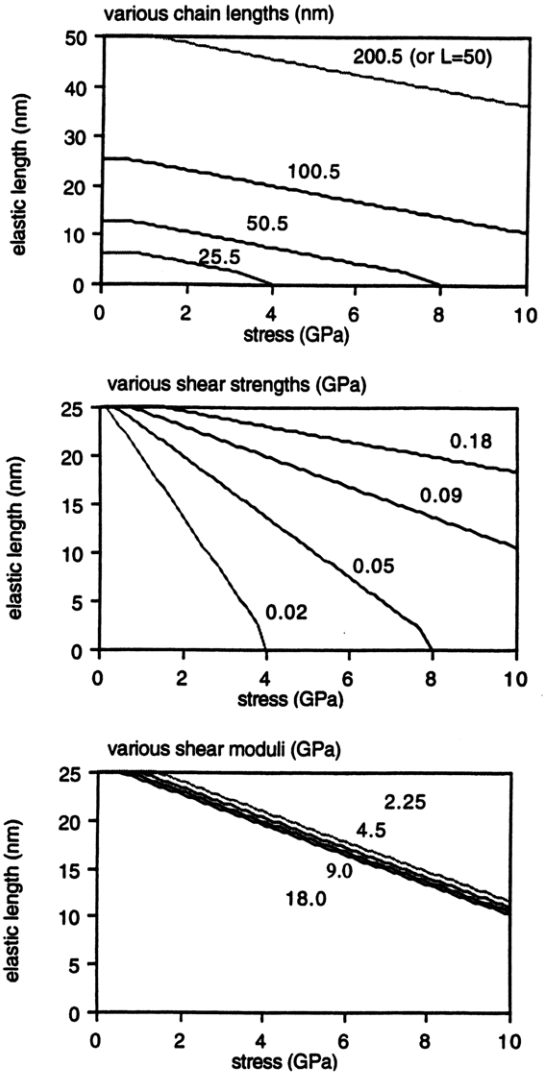

Figure 13. Computed elastic length z_0 as a function of the applied stress, for various chain lengths, shear strengths, and shear moduli. (Unless varied, the defaults values are shear modulus = 9 GPa, shear strength = 0.09 GPa, chain length = 100.5 nm.)

length are respectively 100.5 and 0.5 nm. z_0 decreases from its maximum value to 0 at which point total debonding and chain slip occurs, unless failure by chain scission occurs first. The rate of decrease of the elastic region with increased stress is $dz_0/d\sigma = -1/p\tau_0$ if approximation 14 is right, e.g. when z_0 is not yet close to zero. As seen in Figure 13, this rate is independent of the chain length. Thus chain slip occurs at a lower applied stress for shorter chains because the length available for debonding is shorter. Similarly, the rate

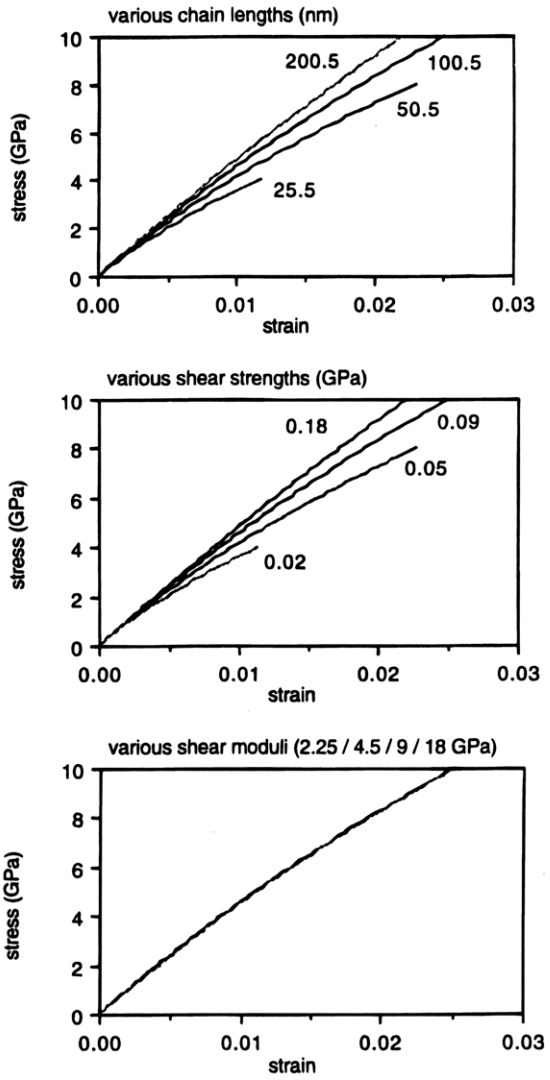

Figure 14. Computed stress–strain curves for various chain lengths, shear strengths, and shear moduli. (Unless varied, the defaults values are shear modulus = 9 GPa, shear strength = 0.09 GPa, chain length = 100.5 nm.)

of decrease of the elastic region with increased stress, $dz_0/d\sigma$, is independent of the shear modulus. z_0 itself depends little on the shear modulus; thus, increasing the shear modulus of the material does not slow down the growth of the debonded length with increased applied stress. Finally, the shear strength plays a major role on the decay of the elastic region with increasing stress. Increasing the shear strength of the material reduces the extent of the debonded region, because debonding starts at a higher stress and because the debonded region grows with increasing stress at a slower rate.

Stress–strain curves obtained for various chain lengths, interchain shear strengths, and interchain shear moduli are shown on Figure 14. The maximum stress of 10 GPa corresponds to the material's failure by chain scission. Variations in the interchain shear modulus modify the elastic tensile modulus, as seen previously, but do not visibly affect the global shape of the stress–strain curves. In contrast, both the chain length and the intermolecular shear strength have considerable influence on the shape of the curves and on the failure modes. Failure occurs by chain slip for the shorter chains and lowest shear strengths, and by chain scission for longer chains and higher shear strengths.

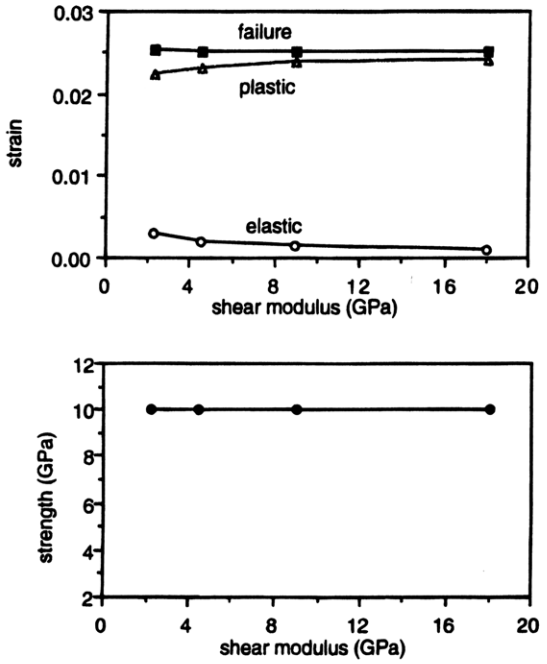

Figure 15. Computed tensile elastic strain, plastic strain, strain to failure, and strength as a function of shear modulus (shear strength = 0.09 GPa, chain length = 100.5 nm).

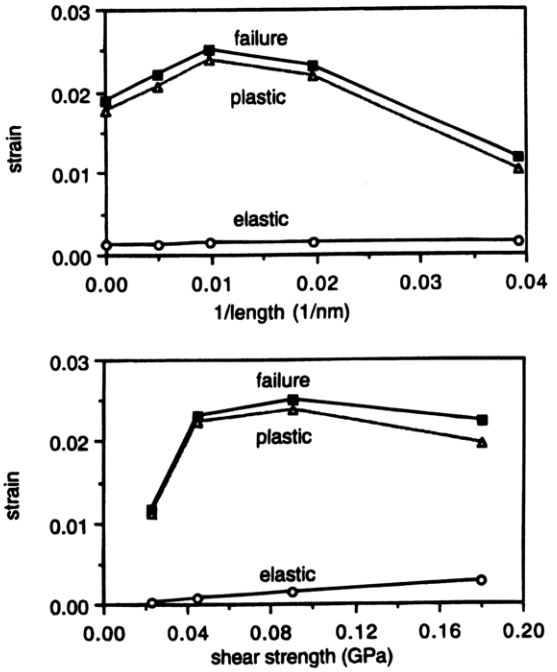

Figure 16. Computed tensile elastic strain, plastic strain, and strain to failure as a function of chain length and shear strength (shear modulus = 9 GPa). (Unless varied, the defaults values are shear strength = 0.09 GPa, chain length = 100.5 nm.)

Such a transition in failure mode has been observed by Penning et al. on cross-linkable high molecular weight polyethylene.[35] The un-cross-linked fibers display a highly fibrillar fracture surface whereas the cross-linked fibers do not show such an extensive fibrillation. Penning points out that the observed difference in fracture morphology between cross-linked and un-cross-linked fibers is not related to a ductile to brittle transition, since the strength and strain at break are almost identical. The observed difference in fracture morphology seems to be related to a chain slip to chain scission transition and may be explained by an increase in shear strength between chains or shearing elements resulting from the cross-linking reaction. A transition in failure mode has also been observed by Termonia et al., in their kinetic approach to the fracture of a perfectly oriented PE fiber.[15] Fracture propagation is due to predominantly intermolecular slippage for low molecular weights and to both slippage and chain scission for higher molecular weights. For PPTA however the failure has been found to be catastrophic chain scission, due to the high stress concentration.[16]

It was shown earlier that an increased interchain shear modulus raises the initial tensile modulus. Yet the shear modulus has little influence on the ultimate properties, as shown on Figure 15. Note, however, that the model assumes a shear modulus and shear strength independent of each other, an assumption not quite correct, as shown by Knoff on torsional experiments of various aramid fibers.[34] In contrast, the molecular length and the intermolecular shear strength both influence the stress and strain to failure considerably, as shown in Figures 16 and 17. The evolution of the elastic and plastic strains and of the strain to failure are plotted in Figure 16 as a function of chain length and interchain shear strength. The debonding phenomenon is important, as emphasized by some interchain debonding or plastic shear being present during most of the deformation. The polymer's strain to failure and strength are predicted for all combinations of shear

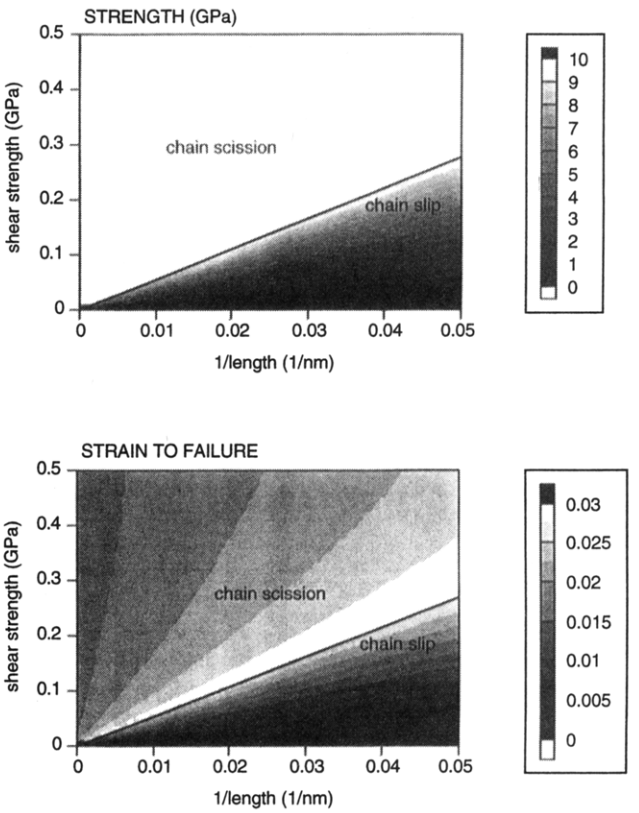

Figure 17. Computed tensile strength and strain to failure as a function of chain length and shear strength (shear modulus = 9 GPa).

strength/chain length on the two-dimensional maps of Figure 17.

At low intermolecular shear strength or for short chains, failure of the polymer occurs by slippage between the chains. In this case longer chains or a higher shear strength will improve both the strength and strain

to failure of the fiber. At higher shear strength or for longer chains, failure occurs because of the rupture of the covalent bonds, before total interchain debonding. Increasing the chain length or the shear strength then has no consequences on the material strength, which only depends on the intrinsic molecular tensile strength. However, the strain to failure is lowered as a result of the higher stiffness and, consequently, the energy to failure decreases for increased chain length and shear strength.

Thus in the molecular engineering of strong, tough oriented polymers, an optimum combination of chain length and shear strength must be chosen. This combination will lead to the highest strength, strain to failure, and toughness and corresponds to failure having the same likelihood to occur by interchain slippage ($\sigma = p\tau_o L$) or chain rupture ($\sigma = \sigma_f/2$), e.g. $\tau_o/\sigma_f = 1/(2pL)$.

The following equation

$$\frac{\tau_o}{\sigma_f} = \frac{1}{2p(2l/4 - a/2)} \approx 4\frac{1}{Z^2}\frac{D}{2l}$$

(with Z being the number of neighbors)

or

$$\frac{\text{interchain shear strength}}{\text{chain tensile strength}} \approx 4\frac{1}{(\text{number of neighbors})^2}\frac{\text{chain dimension}}{\text{chain length}}$$

relates molecular properties for maximum tensile strength and elongation to failure. If we assume that polymers can be synthesized and tailored to a given molecular weight, molecular dimension, chain tensile strength, and interchain shear strength, then this simplified equation indicates how polymers should be made for maximum energy and stress to failure. The more anisotropic the materials properties (low τ_o/σ_f ratio), the higher the aspect ratio (low $D/2l$ ratio) should be to optimize toughness and strength.

Bartenev et al. also found that the dependence of theoretical tensile strength on the molecular weight is related to the strength of the intermolecular interactions.[14] For fully oriented Kapron containing hydrogen bonds, Bartenev shows that failure occurs by chain scission without much slippage, and the molecular length practically exerts no effect on the strength. However for oriented polyethylene or weak intermolecular interaction, the dependence of the strength on chain length is much stronger, and slippage between macromolecules is predicted.

In Yoon's theory of the strength of highly oriented liquid crystal polymers, the tensile strength is proportional to the interchain shear strength.[19] This is similar to our model for a polymer failure by interchain slippage. Yoon's theory assumes that the polymer locally fails when the shear stress exceeds a critical shear strength, and does not take into account simple chain scission. Yoon concludes that any process which increases the shear strength will also increase the polymer tensile strength. In our model, the tensile strength will also rise with increased shear strength but only up to a maximum value.

A linear relationship between the experimentally determined tensile strength and the experimentally determined shear strength was obtained by Knoff for a number of aramid fibers.[34] The hypothesis used to justify these observations was that aramid fiber failure occurs when the shear force at a discontinuity exceeds the shear strength of the bond between the fibrous subcomponents; therefore for the case of elastic shear stress/strain behavior, the tensile strength should be directly proportional to the shear strength. This is similar to the hypothesis and results of our constitutive model for a failure by chain slippage. One difference between our and Knoff's hypotheses resides in the size of the shearing elements, characterized in our model by a size D. For our constitutive model we assume shear between individual molecules, whereas Knoff assumes shear between fibrous subcomponents.

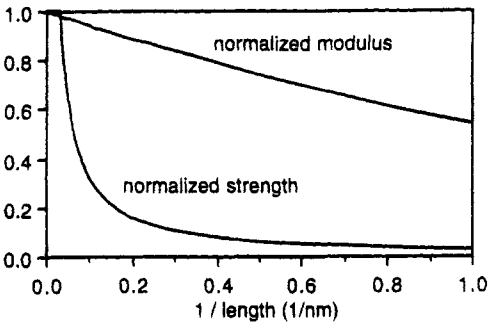

Figure 18. Computed normalized tensile modulus and strength as a function of chain length (shear modulus = 9 GPa, shear strength = 0.09 GPa).

In Termonia et al.'s analysis, the tensile strength increases with molecular weight for both PPTA and PE.[15-17] The drop of the strength with increased chain-end density or inverse of length is sharper for PE than for PPTA. This could be explained by a higher interchain shear strength for PPTA than for PE resulting from the presence of hydrogen bonds.

In a review article on micromechanical modeling of composites, Reifsnider presented a micromechanical model of tensile strength in composite polymer materials.[36] The model is a representation of the balance between two competing effects: the tendency for fiber fractures to join together and lower the bundle strength (low matrix shear strength) and the tendency for broken fibers to break neighboring fibers due to stress concentration effects (high matrix shear strength). The model predicts an optimum value for the matrix shear strength leading to maximum composite strength, corresponding to the balance between low bundle strength and the local stress concentration limitations. These concepts are comparable to those developed here for polymers of oriented macromolecules. With a random chain-end distribution, the tensile stress concentration intensity would not necessarily be 2, and the predicted tensile strength may not plateau but may decrease with increased interchain shear strength for failure by chain scission.

One should note that short molecular lengths are much more detrimental to the strength than to the elastic modulus, as illustrated in Figure 18. The deleterious effect of chain-end defects on tensile strength has been observed before on cross-linkable extended-chain fibers where the cross-linking reaction is thought to be accompanied by chain scission and radical formation.[37,38] In Termonia's modeling data for PE and PPTA, the same trend is observed; e.g. the drop in strength with the inverse of the chain length is sharper than the drop in modulus.[16,17]

In conclusion, the constitutive model described here gives an analytical solution for the tensile response of an ideal chain polymer of finite molecular length. We

show how macroscopic mechanical properties such as tensile strength and elastic modulus may be optimized by changing various intrinsic material parameters. The model describes the mechanical response of an ideal material, which leads to a few simplifications. For example, the polymer contains periodic weak planes perpendicular to the chain axis where the chain ends concentrate, the stress concentration factor is always 2 or the number of neighbors for a given chain, and local shear failure or chain scission becomes a global failure. It is therefore not possible to study the failure initiation and propagation stages independently. Nevertheless the fundamental principles that govern the process of the polymer deformation and fracture are described. More work needs to be done to take into account the random placement of chain ends and the molecular weight distribution.

A numerical solution could easily be applied to various material geometries. In this case failure may occur by slip or by chain scission, and also by both slip and chain scission for intermediate chain lengths and shear strengths. The criteria for failure will be to find a continuous path of broken chains and/or of debonded chains through the material. A numerical solution for the mechanical response of cross-linked oriented polymers could also give insight. The effect of introducing cross-links between the molecules should be to increase the apparent or effective molecular length, change the size of the shearing elements, and/or create a distribution of shear strengths.

(6) Conclusions

•Molecular modeling of periodic crystals of PBZO demonstrates that oriented polymers of extended-chain molecules of finite length are analogous to microcomposites of discontinuous fibers. The local strain distribution along an individual molecule shows that near chain ends, most of the stress is transferred to the nearby chains through a shear lag region via secondary bonds.

•A constitutive model is developed for a geometry similar to the PBZO molecular simulations, for which the molecules of finite length are represented by discontinuous fibers or chains. The calculated strain distribution along the chains of the model is similar to that along the PBZO molecules in molecular simulations. This result shows that elasticity theory may be applied down to the molecular level.

•Raising the value of the intermolecular shear modulus has the same effect as raising the length of the molecular chains for an elastic shear deformation: the stress is transferred over smaller fractions of the chain length at the ends, and the tensile modulus is increased.

•Stress–strain curves are calculated, showing a failure transition from chain scission to chain slip as the chains become shorter or as the intermolecular shear strength is decreased.

•The influence of shear modulus, shear strength, and chain length on material properties such as strength and strain to failure is examined. It is shown that the interchain shear modulus alters the initial elastic modulus but has almost no impact on ultimate properties. However optimum combinations of shear strength/chain tensile modulus ratio and chain aspect ratio lead to maximum strength, strain to failure, and toughness. These optimum conditions correspond to a failure that has the same likelihood to occur by chain slip or by chain rupture, e.g. when the relation

$$\frac{\tau_o}{\sigma_f} = \frac{1}{2p(2l/4 - a/2)} \approx 4\frac{1}{Z^2}\frac{D}{2l}$$

is satisfied. Thus the more anisotropic the materials properties (low τ_o/σ_f ratio), the higher the aspect ratio (low $D/2l$ ratio) should be to optimize toughness and strength.

Acknowledgment. This research was supported by the U.S. Army Advanced Concept Technology Committee (DAAK6-92-K-0005). Generous support was provided from DuPont, Hoechst-Celanese, and the NSF National Young Investigator Program (NSF-DMR-9257569). The authors are grateful to Prof. J. R. Barber (Department of Mechanical Engineering and Applied Mechanics, University of Michigan), and Dr. S. R. Allen (DuPont) for helpful discussions.

References and Notes

(1) Staudinger, H. *Dle Hochmolekularen Organischen Verbindungen*; Verlag Von Julius Springer: Berlin, 1932; p 111.
(2) Yang, H. H. *Aromatic High-Strength Fibers*; Wiley-Interscience: New York, 1989.
(3) Cohen, Y.; Frost, H. H.; Thomas, E. L. Structure Formation and Phase Transformations in Solutions of Rigid Polymers. In *Reversible Polymeric Gels and Related Systems*; Russo, P. S., Ed.; American Chemical Society Symposium Series; American Chemical Society: Washington, DC, 1987; Chapter 12.
(4) Martin, D. C.; Thomas, E. L. Ultrastructure of Poly(*p*-phenylenebenzobis(oxazole) Fibers. *Macromolecules* **1991**, *24*, 2450–2460.
(5) Northolt, M. G.; Van Aartsen, J. J. Chain orientation distribution and elastic properties of poly(p-phenylene terephthalamide), a rigid rod polymer. *J. Polym. Sci.* **1977**, *58*, 283–296.
(6) Northolt, M. G. Tensile deformation of poly(p-phenylene terephthalamide) fibers, an experimental and theoretical analysis. *Polymer* **1980**, *21*, 1999–1204.
(7) Northolt, M. G.; Hout, R. V. D. Elastic extension of an oriented crystalline fiber. *Polymer* **1985**, *26*, 310–316.
(8) Allen, S. R.; Roche, E. J. Deformation behavior of Kevlar aramid fibers. *Polymer* **1989**, *30*, 996–1003.
(9) Penning, J. P.; Van der Werff, H.; Roukema, M.; Pennings, A. J. On the theoretical strength of gel spun/hot drawn ultrahigh molecular weight polyethylene fibers. *Polymer Bull.* **1990**, *23*, 347–352.
(10) Shuppert, A. A. A model for the creep of oriented high-modulus fibers. *Makromol. Chem. Theory Simul.* **1993**, *2*, 643–651.
(11) Martin, D. C. Intermolecular Twist Defects in Extended-Chain Polymers. *Macromolecules* **1992**, *25* (20), 5171–5177.
(12) Predecki, P.; Statton, W. O. Dislocations caused by chain ends in crystalline polymers. *J. Appl. Phys.* **1966**, *37* (11), 4053–4059.
(13) Morgan, R. J.; Pruneda, C. O.; Steele, W. J. The relationship between the physical structure and the macroscopic deformation and failure processes of poly(p-phenylene terephthalamide) fibers. *J. Polym. Sci., Polym. Phys. Ed.* **1983**, *21*, 1757–1783.
(14) Bartenev, G. M.; Valishin, A. A. Theoretical strength of polymers in a completely oriented state. *Mekhanika Polimerov* **1970**, *3*, 458–464.
(15) Termonia, Y.; Meakin, P.; Smith P. Theoretical Study of the Influence of the Molecular Weight on the Maximum Tensile Strength of Polymer Fibers. *Macromolecules* **1985**, *18*, 2246–2252.
(16) Termonia, Y.; Smith, P. Theoretical study of the ultimate mechanical properties of poly(p-phenylene terephthalamide) fibers. *Polymer* **1986**, *27*, 1845–1849.
(17) Termonia, Y.; Smith, P. Effect of chain-end segregation on the theoretical tensile strength of polyethylene and Kevlar. *Polym. Commun.* **1989**, *30*, 66–68.
(18) Termonia, Y. Effect of Size on the Strength of Polymeric Fibers. *J. Polym. Sci., Part B: Polym. Phys.* **1995**, *33*, 147–152.
(19) Yoon, H. N. Strength of fibers from wholly aromatic polyesters. *Colloid Polym. Sci.* **1990**, *268*, 230–239.

(20) Martin, D. C.; Thomas, E. L. *Macromolecules* **1991**, *24* (9), 2450–2460.
(21) Wierschke, S. G. A Computational Study of the Tensile and Compressive Properties of Ordered Polymers via the Austin Model 1 (AM1) Semi-Empirical Orbital Method. Wright-Patterson Air Force Base Report No. AFWAL-TR-88-4201; Wright, Patterson AFB: Dayton, OH, June 1986.
(22) Young, R. J.; Lu, D.; Day, R. J.; Knoff, W. F.; Davis, H. A. Relationship between structure and mechanical properties for aramid fibers. *J. Mater. Sci.* **1992**, *27*, 5431–5440.
(23) Young, R. J.; Yeh, W.-Y. Chain stretching in poly(ethylene-terephthalate) fiber. *Polymer* **1994**, *35* (18), 3844–3847.
(24) Prasad, K.; Grubb, D. T. Deformation behavior of Kevlar fibers studied by Raman spectroscopy. *J. Appl. Polym. Sci.* **1990**, *41*, 2189–2198.
(25) Vlattas, C.; Galiotis, C. Deformation behavior of liquid crystal polymer fibers: 1. Converting spectroscopic data into mechanical stress-strain curves in tension and compression. *Polymer* **1994**, *35* (11), 2335–2347.
(26) Fan, C. F.; Waldman, D. A.; Hsu, S. L. Interfacial effects on stress distribution in model composites. *J. Polym. Sci., Part B: Polym. Phys.* **1991**, *29*, 235–246.
(27) Andrews, M. C.; Young, R. J. Analysis of the deformation of aramid fibers and composites using Raman spectroscopy. *J. Raman Spectrosc.* **1993**, *24*, 539–544.
(28) Andrews, M. C.; Day, R. J.; Patrikis, A. K.; Young, R. J. Deformation micromechanics in aramid/epoxy composites. *Composites* **1994**, *25* (7), 745–751.
(29) Cox, H. L. *J. Appl. Phys.* **1952**, *3*, 72.
(30) Aspden, R. M. Fiber stress and strain in fiber-reinforced composites. *J. Mater. Sci.* **1994**, *29*, 1310–1318.
(31) Gulino, R.; Schwartz, P.; Phoenix, S. L. Experiments on shear deformation, debonding and local load transfer in a model graphite/glass/epoxy microcomposite. *J. Mater. Sci.* **1991**, *26*, 6655–6672.
(32) Ochiai, S.; Hojo, M. Stress distribution in discontinuous fibers in a model composite. *J. Mater. Sci.* **1994**, *29*, 2754–2760.
(33) Kausch, H. H. *Polymer Fracture*; Springer-Verlag: Berlin, Heidelberg, New York, 1978; pp 103–104.
(34) Knoff, W. F.; Relationship between the tensile and shear strength of aramid fibers. *J. Mater. Sci. Lett.* **1987**, *6*, 1392–1394.
(35) Penning, J. P.; Pras, H. E.; Pennings, A. J. Influence of chemical crosslinking on the creep behavior of ultra-high molecular weight polyethylene fibers. *Colloid Polym. Sci.* **1994**, *272* (6), 664–676.
(36) Reifsnider, K. L. Micromechanical modelling of polymeric composites. *Polymer* **1994**, *35* (23), 5035–5040.
(37) Glomm, B.; Rickert, C.; Neuenschwander, P.; Suter, U. W. Thermal crosslinked rigid-rods aramids, 2, fiber spinning and fiber properties. *Macromol. Chem. Phys.* **1994**, *195*, 511–524.
(38) Jiang, T.; Rigney, J.; Jones, M-C. G.; Markoski, L. J.; Spilman, G. E.; Mielewski, D.; Martin, D. C. Processing and characterization of Thermally Cross-Linkable PPTA-*co*-XTA Copolymers. *Macromolecules* **1995**, *28*, 3301–3312.

MA950163L